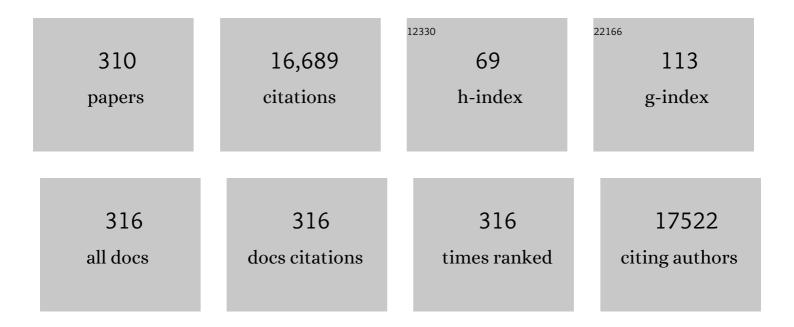
List of Publications by Year in descending order

Source: https://exaly.com/author-pdf/5554167/publications.pdf Version: 2024-02-01



#	Article	IF	CITATIONS
1	Efficient Visible-Light Photocatalytic Hydrogen Evolution and Enhanced Photostability of Core/Shell CdS/g-C ₃ N ₄ Nanowires. ACS Applied Materials & Interfaces, 2013, 5, 10317-10324.	8.0	747
2	Progress of nanocrystalline growth kinetics based on oriented attachment. Nanoscale, 2010, 2, 18-34.	5.6	486
3	SnS nanoparticles electrostatically anchored on three-dimensional N-doped graphene as an active and durable anode for sodium-ion batteries. Energy and Environmental Science, 2017, 10, 1757-1763.	30.8	431
4	Noble metal-free Ni(OH)2–g-C3N4 composite photocatalyst with enhanced visible-light photocatalytic H2-production activity. Catalysis Science and Technology, 2013, 3, 1782.	4.1	411
5	Nickel Metal–Organic Framework Monolayers for Photoreduction of Diluted CO ₂ : Metalâ€Nodeâ€Dependent Activity and Selectivity. Angewandte Chemie - International Edition, 2018, 57, 16811-16815.	13.8	387
6	Investigation of the interaction between acridine orange and bovine serum albumin. Talanta, 1998, 47, 1223-1229.	5.5	367
7	Iron phthalocyanine with coordination induced electronic localization to boost oxygen reduction reaction. Nature Communications, 2020, 11, 4173.	12.8	358
8	Powerful uranium extraction strategy with combined ligand complexation and photocatalytic reduction by postsynthetically modified photoactive metal-organic frameworks. Applied Catalysis B: Environmental, 2019, 254, 47-54.	20.2	222
9	Enhanced Photocatalytic Hydrogen Production Activities of Au-Loaded ZnS Flowers. ACS Applied Materials & Interfaces, 2013, 5, 1031-1037.	8.0	221
10	CoSe ₂ Nanoparticles Encapsulated by Nâ€Doped Carbon Framework Intertwined with Carbon Nanotubes: Highâ€Performance Dualâ€Role Anode Materials for Both Li―and Naâ€Ion Batteries. Advanced Science, 2018, 5, 1800763.	11.2	215
11	MOFs-derived ultrathin holey Co3O4 nanosheets for enhanced visible light CO2 reduction. Applied Catalysis B: Environmental, 2019, 244, 996-1003.	20.2	207
12	Mg(OH) ₂ Supported Nanoscale Zero Valent Iron Enhancing the Removal of Pb(II) from Aqueous Solution. ACS Applied Materials & Interfaces, 2015, 7, 7961-7969.	8.0	198
13	Insights into the activity of single-atom Fe-N-C catalysts for oxygen reduction reaction. Nature Communications, 2022, 13, 2075.	12.8	197
14	A Multistep Oriented Attachment Kinetics:Â Coarsening of ZnS Nanoparticle in Concentrated NaOH. Journal of the American Chemical Society, 2006, 128, 12981-12987.	13.7	194
15	DNA Attachment and Hybridization at the Silicon (100) Surface. Langmuir, 2002, 18, 788-796.	3.5	190
16	Investigation of Antibacterial Activity and Related Mechanism of a Series of Nano-Mg(OH) ₂ . ACS Applied Materials & Interfaces, 2013, 5, 1137-1142.	8.0	185
17	Growth Strategy and Physical Properties of the High Mobility P-Type CuI Crystal. Crystal Growth and Design, 2010, 10, 2057-2060.	3.0	176
18	Treatment of Cr ^{VI} â€Containing Mg(OH) ₂ Nanowaste. Angewandte Chemie - International Edition, 2008, 47, 5619-5622.	13.8	175

#	Article	IF	CITATIONS
19	Effective Extraction of Cr(VI) from Hazardous Gypsum Sludge via Controlling the Phase Transformation and Chromium Species. Environmental Science & Technology, 2018, 52, 13336-13342.	10.0	175
20	Recent progress in understanding the mechanism of heavy metals retention by iron (oxyhydr)oxides. Science of the Total Environment, 2021, 752, 141930.	8.0	172
21	Recycling Rare Earth Elements from Industrial Wastewater with Flowerlike Nano-Mg(OH) ₂ . ACS Applied Materials & Interfaces, 2013, 5, 9719-9725.	8.0	171
22	Crystal growth by oriented attachment: kinetic models and control factors. CrystEngComm, 2014, 16, 1419.	2.6	162
23	Recycling Mg(OH) ₂ Nanoadsorbent during Treating the Low Concentration of Cr ^{VI} . Environmental Science & Technology, 2011, 45, 1955-1961.	10.0	153
24	Heterointerface Engineering of Hierarchical Bi ₂ S ₃ /MoS ₂ with Selfâ€Generated Rich Phase Boundaries for Superior Sodium Storage Performance. Advanced Functional Materials, 2020, 30, 1910732.	14.9	151
25	Enhanced Adsorption of <i>p</i> -Arsanilic Acid from Water by Amine-Modified UiO-67 as Examined Using Extended X-ray Absorption Fine Structure, X-ray Photoelectron Spectroscopy, and Density Functional Theory Calculations. Environmental Science & Technology, 2018, 52, 3466-3475.	10.0	148
26	Accelerating CO ₂ Electroreduction to Multicarbon Products via Synergistic Electric–Thermal Field on Copper Nanoneedles. Journal of the American Chemical Society, 2022, 144, 3039-3049.	13.7	147
27	ZnS nano-architectures: photocatalysis, deactivation and regeneration. Nanoscale, 2010, 2, 2062.	5.6	146
28	Ultrathin Co-Co LDHs nanosheets assembled vertically on MXene: 3D nanoarrays for boosted visible-light-driven CO2 reduction. Chemical Engineering Journal, 2020, 391, 123519.	12.7	142
29	Different Pathways for Cr(III) Oxidation: Implications for Cr(VI) Reoccurrence in Reduced Chromite Ore Processing Residue. Environmental Science & Technology, 2020, 54, 11971-11979.	10.0	141
30	Upcycling of Electroplating Sludge into Ultrafine Sn@C Nanorods with Highly Stable Lithium Storage Performance. Nano Letters, 2019, 19, 1860-1866.	9.1	139
31	Migration and potential risk of trace phthalates in bottled water: AÂglobal situation. Water Research, 2018, 147, 362-372.	11.3	134
32	Bisphenol A concentrations in human urine, human intakes across six continents, and annual trends of average intakes in adult and child populations worldwide: A thorough literature review. Science of the Total Environment, 2018, 626, 971-981.	8.0	133
33	Bioremediation of Cr(VI) and Immobilization as Cr(III) by <i>Ochrobactrum anthropi</i> . Environmental Science & Technology, 2010, 44, 6357-6363.	10.0	130
34	Biomineralization of Pb(II) into Pb-hydroxyapatite induced by Bacillus cereus 12-2 isolated from Lead–Zinc mine tailings. Journal of Hazardous Materials, 2016, 301, 531-537.	12.4	121
35	Synergy between Plasmonic and Electrocatalytic Activation of Methanol Oxidation on Palladium–Silver Alloy Nanotubes. Angewandte Chemie - International Edition, 2019, 58, 8794-8798.	13.8	120
36	Experimental and theoretical calculation investigation on efficient Pb(<scp>ii</scp>) adsorption on etched Ti ₃ AlC ₂ nanofibers and nanosheets. Environmental Science: Nano, 2018, 5, 946-955.	4.3	118

#	Article	IF	CITATIONS
37	Investigation of Cr(VI) reduction and Cr(III) immobilization mechanism by planktonic cells and biofilms of Bacillus subtilis ATCC-6633. Water Research, 2014, 55, 21-29.	11.3	116
38	Kinetics of Cation and Oxyanion Adsorption and Desorption on Ferrihydrite: Roles of Ferrihydrite Binding Sites and a Unified Model. Environmental Science & Technology, 2017, 51, 10605-10614.	10.0	115
39	A study of the potential application of nano-Mg(OH)2 in adsorbing low concentrations of uranyl tricarbonate from water. Nanoscale, 2012, 4, 2423.	5.6	111
40	ZnO nanoflower-based photoelectrochemical DNAzyme sensor for the detection of Pb2+. Biosensors and Bioelectronics, 2014, 56, 243-249.	10.1	109
41	Surface Amorphization of Vanadium Dioxide (B) for Kâ€ l on Battery. Advanced Energy Materials, 2020, 10, 2000717.	19.5	109
42	Enhanced visible light photocatalytic hydrogen production activity of CuS/ZnS nanoflower spheres. Journal of Materials Chemistry A, 2015, 3, 13913-13919.	10.3	108
43	Schottky or Ohmic Metal–Semiconductor Contact: Influence on Photocatalytic Efficiency of Ag/ZnO and Pt/ZnO Model Systems. ChemSusChem, 2014, 7, 101-104.	6.8	103
44	A novel magnetically separable TiO2/CoFe2O4 nanofiber with high photocatalytic activity under UV–vis light. Materials Research Bulletin, 2012, 47, 333-337.	5.2	101
45	Hierarchical NiCo2O4 hollow nanocages for photoreduction of diluted CO2: Adsorption and active sites engineering. Applied Catalysis B: Environmental, 2020, 260, 118208.	20.2	101
46	Trace determination of sulfonamide antibiotics and their acetylated metabolites via SPE-LC-MS/MS in wastewater and insights from their occurrence in a municipal wastewater treatment plant. Science of the Total Environment, 2019, 653, 815-821.	8.0	99
47	CoSe@N-Doped Carbon Nanotubes as a Potassium-Ion Battery Anode with High Initial Coulombic Efficiency and Superior Capacity Retention. ACS Nano, 2021, 15, 1121-1132.	14.6	98
48	FeOOH-loaded MnO2 nano-composite: An efficient emergency material for thallium pollution incident. Journal of Environmental Management, 2017, 192, 31-38.	7.8	97
49	MgZnO-based metal-semiconductor-metal solar-blind photodetectors on ZnO substrates. Applied Physics Letters, 2011, 98, 221112.	3.3	96
50	Drivers and applications of integrated clean-up technologies for surfactant-enhanced remediation of environments contaminated with polycyclic aromatic hydrocarbons (PAHs). Environmental Pollution, 2017, 225, 129-140.	7.5	95
51	Kinetics of heavy metal adsorption and desorption in soil: Developing a unified model based on chemical speciation. Geochimica Et Cosmochimica Acta, 2018, 224, 282-300.	3.9	93
52	The removal of heavy metal cations by sulfidated nanoscale zero-valent iron (S-nZVI): The reaction mechanisms and the role of sulfur. Journal of Hazardous Materials, 2021, 404, 124057.	12.4	93
53	The observation of the local ordering characteristics of spermidine- condensed DNA: atomic force microscopy and polarizing microscopy studies. Nucleic Acids Research, 1998, 26, 3228-3234.	14.5	91
54	Kinetics of Heavy Metal Dissociation from Natural Organic Matter: Roles of the Carboxylic and Phenolic Sites. Environmental Science & Technology, 2016, 50, 10476-10484.	10.0	91

#	Article	IF	CITATIONS
55	Zeolite A synthesized from alkaline assisted pre-activated halloysite for efficient heavy metal removal in polluted river water and industrial wastewater. Journal of Environmental Sciences, 2017, 56, 254-262.	6.1	91
56	2D–2D Heterostructured UNiMOF/g-C ₃ N ₄ for Enhanced Photocatalytic H ₂ Production under Visible-Light Irradiation. ACS Sustainable Chemistry and Engineering, 2019, 7, 2492-2499.	6.7	90
57	Enhanced removal of roxarsone by Fe ₃ O ₄ @3D graphene nanocomposites: synergistic adsorption and mechanism. Environmental Science: Nano, 2017, 4, 2134-2143.	4.3	89
58	A convenient method of aligning large DNA molecules on bare mica surfaces for atomic force microscopy. Nucleic Acids Research, 1998, 26, 4785-4786.	14.5	81
59	Surface Chemistry Controls Crystallinity of ZnS Nanoparticles. Nano Letters, 2006, 6, 605-610.	9.1	80
60	Cr(VI) uptake mechanism of Bacillus cereus. Chemosphere, 2012, 87, 211-216.	8.2	80
61	Potentially toxic elements in solid waste streams: Fate and management approaches. Environmental Pollution, 2019, 253, 680-707.	7.5	79
62	The double influence mechanism of pH on arsenic removal by nano zero valent iron: electrostatic interactions and the corrosion of Fe ⁰ . Environmental Science: Nano, 2017, 4, 1544-1552.	4.3	78
63	Microscopic Investigations of the Cr(VI) Uptake Mechanism of Living <i>Ochrobactrum anthropi</i> . Langmuir, 2008, 24, 9630-9635.	3.5	77
64	Hydrothermal Growth of ZnO Single Crystals with High Carrier Mobility. Crystal Growth and Design, 2009, 9, 4378-4383.	3.0	77
65	High levels of microplastic pollution in aquaculture water of fish ponds in the Pearl River Estuary of Guangzhou, China. Science of the Total Environment, 2020, 744, 140679.	8.0	77
66	Simultaneous removal of Cu(II) and Cr(VI) by Mg–Al–Cl layered double hydroxide and mechanism insight. Journal of Environmental Sciences, 2017, 53, 16-26.	6.1	76
67	Chemical Modification and Patterning of Iodine-Terminated Silicon Surfaces Using Visible Light. Journal of Physical Chemistry B, 2002, 106, 2656-2664.	2.6	74
68	Tailoring the crystal forms of the Ni-MOF catalysts for enhanced photocatalytic CO2-to-CO performance. Applied Catalysis B: Environmental, 2022, 309, 121232.	20.2	74
69	Targeted conversion of Ni in electroplating sludge to nickel ferrite nanomaterial with stable lithium storage performance. Journal of Hazardous Materials, 2020, 393, 122296.	12.4	73
70	Oriented Attachment Kinetics for Ligand Capped Nanocrystals:Â Coarsening of Thiol-PbS Nanoparticles. Journal of Physical Chemistry B, 2007, 111, 1449-1454.	2.6	68
71	3D spatially branched hierarchical Z-scheme CdS-Au nanoclusters-ZnO hybrids with boosted photocatalytic hydrogen evolution. Journal of Alloys and Compounds, 2018, 754, 105-113.	5.5	68
72	Sb/C composite as a high-performance anode for sodium ion batteries. Electrochimica Acta, 2017, 242, 159-164.	5.2	67

#	Article	IF	CITATIONS
73	Biogenic Calcium Carbonate with Hierarchical Organic–Inorganic Composite Structure Enhancing the Removal of Pb(II) from Wastewater. ACS Applied Materials & Interfaces, 2017, 9, 35785-35793.	8.0	67
74	Vacancy engineering in nanostructured semiconductors for enhancing photocatalysis. Journal of Materials Chemistry A, 2021, 9, 17143-17172.	10.3	66
75	Strategy for Preparing Al-Doped ZnO Thin Film with High Mobility and High Stability. Crystal Growth and Design, 2011, 11, 21-25.	3.0	65
76	Influence of lattice integrity and phase composition on the photocatalytic hydrogen production efficiency of ZnS nanomaterials. Nanoscale, 2012, 4, 2859.	5.6	65
77	General and Scalable Fabrication of Core–Shell Metal Sulfides@C Anchored on 3D Nâ€Đoped Foam toward Flexible Sodium Ion Batteries. Small, 2019, 15, e1903259.	10.0	62
78	The mechanism of uranium transformation from U(VI) into nano-uramphite by two indigenous Bacillus thuringiensis strains. Journal of Hazardous Materials, 2015, 297, 313-319.	12.4	61
79	Ferrihydrite transformation under the impact of humic acid and Pb: kinetics, nanoscale mechanisms, and implications for C and Pb dynamics. Environmental Science: Nano, 2019, 6, 747-762.	4.3	59
80	Mechanism of As(V) removal by green synthesized iron nanoparticles. Journal of Hazardous Materials, 2019, 379, 120811.	12.4	59
81	EDTA-Induced Self-Assembly of 3D Graphene and Its Superior Adsorption Ability for Paraquat Using a Teabag. ACS Applied Materials & Interfaces, 2014, 6, 19766-19773.	8.0	58
82	Aggregation-Induced Fast Crystal Growth of SnO ₂ Nanocrystals. Journal of the American Chemical Society, 2012, 134, 16228-16234.	13.7	57
83	Melamine-assisted synthesis of Fe ₃ N featuring highly reversible crystalline-phase transformation for ultrastable sodium ion storage. Journal of Materials Chemistry A, 2020, 8, 6768-6775.	10.3	57
84	Global review of phthalates in edible oil: An emerging and nonnegligible exposure source to human. Science of the Total Environment, 2020, 704, 135369.	8.0	56
85	Correlation between the Photoluminescence and Oriented Attachment Growth Mechanism of CdS Quantum Dots. Journal of the American Chemical Society, 2010, 132, 9528-9530.	13.7	54
86	Remediation of Chromium and Uranium Contamination by Microbial Activity. Elements, 2012, 8, 107-112.	0.5	54
87	Nickel Metal–Organic Framework Monolayers for Photoreduction of Diluted CO ₂ : Metalâ€Nodeâ€Dependent Activity and Selectivity. Angewandte Chemie, 2018, 130, 17053-17057.	2.0	54
88	Pure multistep oriented attachment growth kinetics of surfactant-free SnO2 nanocrystals. Physical Chemistry Chemical Physics, 2009, 11, 8516.	2.8	53
89	A Thermodynamically Stable Nanophase Material. Journal of the American Chemical Society, 2006, 128, 6126-6131.	13.7	52
90	Effective capture of aqueous uranium from saline lake with magnesium-based binary and ternary lavered double bydroxides. Science of the Total Environment, 2019, 677, 556-563	8.0	51

#	Article	IF	CITATIONS
91	Research progress in ZnO single-crystal: growth, scientific understanding, and device applications. Science Bulletin, 2014, 59, 1235-1250.	1.7	50
92	Photocatalytic debromination of polybrominated diphenyl ethers (PBDEs) on metal doped TiO2 nanocomposites: Mechanisms and pathways. Environment International, 2019, 127, 5-12.	10.0	49
93	Boosted photoreduction of diluted CO2 through oxygen vacancy engineering in NiO nanoplatelets. Nano Research, 2021, 14, 730-737.	10.4	49
94	Defective magnesium ferrite nano-platelets for the adsorption of As(V): The role of surface hydroxyl groups. Environmental Pollution, 2018, 235, 11-19.	7.5	46
95	Preparation of sludge biochar rich in carboxyl/hydroxyl groups by quenching process and its excellent adsorption performance for Cr(VI). Chemosphere, 2021, 285, 131439.	8.2	46
96	Adsorption-Induced Crystallization of U-Rich Nanocrystals on Nano-Mg(OH) ₂ and the Aqueous Uranyl Enrichment. ACS Applied Materials & Interfaces, 2014, 6, 1301-1305.	8.0	45
97	Catalytic hydrodechlorination of triclosan using a new class of anion-exchange-resin supported palladium catalysts. Water Research, 2017, 120, 199-210.	11.3	45
98	A Quantitative Model for the Coupled Kinetics of Arsenic Adsorption/Desorption and Oxidation on Manganese Oxides. Environmental Science and Technology Letters, 2018, 5, 175-180.	8.7	44
99	Immobilization of cadmium in contaminated soils using sulfidated nanoscale zero-valent iron: Effectiveness and remediation mechanism. Journal of Hazardous Materials, 2021, 420, 126605.	12.4	44
100	Friction Coefficients Derived from Apparent Height Variations in Contact Mode Atomic Force Microscopy Images. Langmuir, 1999, 15, 7662-7669.	3.5	43
101	Biomineralization mechanism of U(VI) induced by Bacillus cereus 12-2: The role of functional groups and enzymes. Chemosphere, 2018, 206, 682-692.	8.2	43
102	Mechanisms and pathways of debromination of polybrominated diphenyl ethers (PBDEs) in various nano-zerovalent iron-based bimetallic systems. Science of the Total Environment, 2019, 661, 18-26.	8.0	42
103	Effect of Surface Etching on the Efficiency of ZnO-Based Dye-Sensitized Solar Cells. Langmuir, 2010, 26, 7153-7156.	3.5	41
104	Paramagnetic anisotropy of Co-doped ZnO single crystal. Applied Physics Letters, 2006, 89, 112507.	3.3	40
105	A Rapid and Robust Light-and-Solution-Triggered In Situ Crafting of Organic Passivating Membrane over Metal Halide Perovskites for Markedly Improved Stability and Photocatalysis. Nano Letters, 2021, 21, 1643-1650.	9.1	40
106	Insights into CO2 adsorption on KOH-activated biochars derived from the mixed sewage sludge and pine sawdust. Science of the Total Environment, 2022, 826, 154133.	8.0	40
107	Reversible Switch between Bulk MgCO ₃ ·3H ₂ O and Mg(OH) ₂ Micro/Nanorods Induces Continuous Selective Preconcentration of Anionic Dyes. ACS Applied Materials & Interfaces, 2013, 5, 7698-7703.	8.0	39
108	Rational Design of FeNi Bimetal Modified Covalent Organic Frameworks for Photoconversion of Anthropogenic CO ₂ into Widely Tunable Syngas. Small, 2020, 16, e2002985.	10.0	39

#	ARTICLE	IF	CITATIONS
109	Real-time molecular monitoring of chemical environment in obligate anaerobes during oxygen adaptive response. Proceedings of the National Academy of Sciences of the United States of America, 2009, 106, 12599-12604.	7.1	38
110	Use of High-Pressure CO ₂ for Concentrating Cr ^{VI} from Electroplating Wastewater by Mg–Al Layered Double Hydroxide. ACS Applied Materials & Interfaces, 2013, 5, 11271-11275.	8.0	38
111	Removal of Sb(III) from wastewater by magnesium oxide and the related mechanisms. Environmental Research, 2020, 186, 109489.	7.5	38
112	Photoconversion of anthropogenic CO2 into tunable syngas over industrial wastes derived metal-organic frameworks. Applied Catalysis B: Environmental, 2021, 283, 119594.	20.2	38
113	High-efficiency adsorption of Cr(VI) and RhB by hierarchical porous carbon prepared from coal gangue. Chemosphere, 2021, 275, 130008.	8.2	38
114	Growth and Phase-Transformation Mechanisms of Nanocrystalline CdS in Na ₂ S Solution. Journal of Physical Chemistry C, 2008, 112, 9229-9233.	3.1	37
115	Tunable surface charge of ZnS : Cu nano-adsorbent induced the selective preconcentration of cationic dyes from wastewater. Nanoscale, 2012, 4, 3665.	5.6	37
116	Facile synthesis of recycling Fe3O4/graphene adsorbents with potassium humate for Cr(VI) removal. Colloids and Surfaces A: Physicochemical and Engineering Aspects, 2019, 560, 384-392.	4.7	37
117	Identification of the key host phases of Cr in fresh chromite ore processing residue (COPR). Science of the Total Environment, 2020, 703, 135075.	8.0	37
118	Study of interface electric field affecting the photocatalysis of ZnO. Chemical Communications, 2011, 47, 4517.	4.1	35
119	Fabrication of titanium phosphate@graphene oxide nanocomposite and its super performance on Eu ³⁺ recycling. Journal of Materials Chemistry A, 2014, 2, 14979-14985.	10.3	35
120	Template-synthesized ultra-thin molecularly imprinted polymers membrane for the selective preconcentration of dyes. Journal of Materials Chemistry A, 2015, 3, 10959-10968.	10.3	35
121	Insight into the roles of endogenous minerals in the activation of persulfate by graphitized biochar for tetracycline removal. Science of the Total Environment, 2021, 768, 144281.	8.0	35
122	Engineering Ultrafine NiFeâ€LDH into Selfâ€Supporting Nanosheets: Separationâ€andâ€Reunion Strategy to Expose Additional Edge Sites for Oxygen Evolution. Small, 2021, 17, e2103785.	10.0	35
123	Evolution of ZnS Nanostructure Morphology under Interfacial Free-Energy Control. Chemistry of Materials, 2008, 20, 2438-2443.	6.7	34
124	Treatment of nanowaste via fast crystal growth: With recycling of nano-SnO2 from electroplating sludge as a study case. Journal of Hazardous Materials, 2012, 211-212, 414-419.	12.4	34
125	[Ru(bpy) 3] 2+ -mediated photoelectrochemical detection of bisphenol A on a molecularly imprinted polypyrrole modified SnO 2 electrode. Analytica Chimica Acta, 2015, 887, 59-66.	5.4	34
126	Dopamine adsorption precursor enables N-doped carbon sheathing of MoS2 nanoflowers for all-around enhancement of supercapacitor performance. Journal of Alloys and Compounds, 2017, 693, 955-963.	5.5	34

#	Article	IF	CITATIONS
127	Fast trace determination of nine odorant and estrogenic chloro- and bromo-phenolic compounds in real water samples through automated solid-phase extraction coupled with liquid chromatography tandem mass spectrometry. Environmental Science and Pollution Research, 2018, 25, 3813-3822.	5.3	34
128	Coupled Kinetics of Ferrihydrite Transformation and As(V) Sequestration under the Effect of Humic Acids: A Mechanistic and Quantitative Study. Environmental Science & Technology, 2018, 52, 11632-11641.	10.0	34
129	Synthesis of CoFe2O4/C nano-catalyst with excellent performance by molten salt method and its application in 4-nitrophenol reduction. Environmental Pollution, 2019, 254, 112961.	7.5	34
130	Synthesis of NiFeAl LDHs from electroplating sludge and Their excellent supercapacitor performance. Journal of Hazardous Materials, 2021, 404, 124113.	12.4	34
131	"In-situ synthesized―iron-based bimetal promotes efficient removal of Cr(VI) in by zero-valent iron-loaded hydroxyapatite. Journal of Hazardous Materials, 2021, 420, 126540.	12.4	34
132	PCN-224/rGO nanocomposite based photoelectrochemical sensor with intrinsic recognition ability for efficient <i>p</i> -arsanilic acid detection. Environmental Science: Nano, 2019, 6, 207-215.	4.3	33
133	Adsorption of low-concentration mercury in water by 3D cyclodextrin/graphene composites: Synergistic effect and enhancement mechanism. Environmental Pollution, 2019, 252, 1133-1141.	7.5	33
134	Preparation of 2D nitrogen-doped magnetic Fe3C/C by in-situ self-assembled double-template method for enhanced removal of Cr(VI). Environmental Pollution, 2020, 263, 114374.	7.5	33
135	A highly efficient photoelectrochemical sensor for detection of chlorpyrifos based on 2D/2D β-Bi ₂ O ₃ /g-C ₃ N ₄ heterojunctions. Environmental Science: Nano, 2021, 8, 773-783.	4.3	33
136	NaOH Concentration Effect on the Oriented Attachment Growth Kinetics of ZnS. Journal of Physical Chemistry B, 2007, 111, 5290-5294.	2.6	32
137	Mn ₂ O ₃ hollow spheres synthesized based on an ion-exchange strategy from amorphous calcium carbonate for highly efficient trace-level uranyl extraction. Environmental Science: Nano, 2016, 3, 1254-1258.	4.3	32
138	Mussel-inspired functionalization of biological calcium carbonate for improving Eu(III) adsorption and the related mechanisms. Chemical Engineering Journal, 2018, 351, 816-824.	12.7	32
139	The effects of interaction between vermiculite and manganese dioxide on the environmental geochemical process of thallium. Science of the Total Environment, 2019, 669, 903-910.	8.0	32
140	Efficient removal of iron from red gypsum via synergistic regulation of gypsum phase transformation and iron speciation. Science of the Total Environment, 2021, 791, 148319.	8.0	32
141	The growth and investigation on Ga-doped ZnO single crystals with high thermal stability and high carrier mobility. CrystEngComm, 2011, 13, 3338.	2.6	31
142	Emerging investigator series: treatment and recycling of heavy metals from nanosludge. Environmental Science: Nano, 2019, 6, 1657-1673.	4.3	31
143	Identification of Cr(VI) speciation in ferrous sulfate-reduced chromite ore processing residue (rCOPR) and impacts of environmental factors erosion on Cr(VI) leaching. Journal of Hazardous Materials, 2019, 373, 389-396.	12.4	31
144	Biomimetic inspired porphyrin-based nanoframes for highly efficient photocatalytic CO2 reduction. Chemical Engineering Journal, 2021, 411, 128414.	12.7	31

#	Article	IF	CITATIONS
145	Accelerated Degradation of Microplastics at the Liquid Interface of Ice Crystals in Frozen Aqueous Solutions. Angewandte Chemie - International Edition, 2022, 61, .	13.8	31
146	Coupled Kinetics Model for Microbially Mediated Arsenic Reduction and Adsorption/Desorption on Iron Oxides: Role of Arsenic Desorption Induced by Microbes. Environmental Science & Technology, 2019, 53, 8892-8902.	10.0	30
147	Rapid debromination of polybrominated diphenyl ethers (PBDEs) by zero valent metal and bimetals: Mechanisms and pathways assisted by density function theory calculation. Environmental Pollution, 2018, 240, 745-753.	7.5	29
148	Efficient removal of low-concentration organoarsenic by Zr-based metal–organic frameworks: cooperation of defects and hydrogen bonds. Environmental Science: Nano, 2019, 6, 3590-3600.	4.3	29
149	Solidification/stabilization of highly toxic arsenic-alkali residue by MSWI fly ash-based cementitious material containing Friedel's salt: Efficiency and mechanism. Journal of Hazardous Materials, 2022, 425, 127992.	12.4	29
150	Identification and characterization of the chromium(VI) responding protein from a newly isolated Ochrobactrum anthropi CTS-325. Journal of Environmental Sciences, 2009, 21, 1673-1678.	6.1	28
151	Remediation of soil and groundwater contaminated with organic chemicals using stabilized nanoparticles: Lessons from the past two decades. Frontiers of Environmental Science and Engineering, 2020, 14, 1.	6.0	28
152	The Effects of Particle Concentration and Surface Charge on the Oriented Attachment Growth Kinetics of CdTe Nanocrystals in H ₂ O. Journal of Physical Chemistry C, 2011, 115, 10357-10364.	3.1	27
153	Dynamic Behavior of Interfacial Water on Mg(OH) ₂ (001) Surface: A Molecular Dynamics Simulation Work. Journal of Physical Chemistry C, 2014, 118, 29887-29895.	3.1	27
154	Interfacial Engineering Improved the Selective Extraction of Uranyl from Saline Water by Nano-Mg(OH) ₂ and the Underlying Mechanism. ACS Sustainable Chemistry and Engineering, 2016, 4, 801-809.	6.7	27
155	Surface defects enhance the adsorption affinity and selectivity of Mg(OH) ₂ towards As(<scp>v</scp>) and Cr(<scp>vi</scp>) oxyanions: a combined theoretical and experimental study. Environmental Science: Nano, 2018, 5, 2570-2578.	4.3	27
156	Fe ₂ P-decorated N,P Codoped Carbon Synthesized via Direct Biological Recycling for Endurable Sulfur Encapsulation. ACS Central Science, 2020, 6, 1827-1834.	11.3	27
157	One-step extraction of high-purity CuCl2·2H2O from copper-containing electroplating sludge based on the directional phase conversion. Journal of Hazardous Materials, 2021, 413, 125469.	12.4	27
158	The high efficient Sb(III) removal by cauliflower like amorphous nanoscale zero-valent iron (A-nZVI). Journal of Hazardous Materials, 2022, 436, 129056.	12.4	27
159	Ultraviolet-light-induced bactericidal mechanism on ZnO single crystals. Chemical Communications, 2009, , 6783.	4.1	26
160	Nanoadduct relieves: Alleviation of developmental toxicity of Cr(VI) due to its spontaneous adsorption to Mg(OH)2 nanoflakes. Journal of Hazardous Materials, 2015, 287, 296-305.	12.4	26
161	Molecular fractionation and sub-nanoscale distribution of dissolved organic matter on allophane. Environmental Science: Nano, 2019, 6, 2037-2048.	4.3	26
162	Ruthenium Nanoparticles Supported on Mg(OH) ₂ Microflowers as Catalysts for Photothermal Carbon Dioxide Hydrogenation. ACS Applied Nano Materials, 2020, 3, 3028-3033.	5.0	25

#	Article	IF	CITATIONS
163	An Overlooked Natural Hydrogen Evolution Pathway: Ni ²⁺ Boosting H ₂ O Reduction by Fe(OH) ₂ Oxidation during Lowâ€Temperature Serpentinization. Angewandte Chemie - International Edition, 2021, 60, 24054-24058.	13.8	25
164	Efficient stabilization of arsenic in the arsenic-bearing lime-ferrate sludge by zero valent iron-enhanced hydrothermal treatment. Chemical Engineering Journal, 2021, 421, 129683.	12.7	25
165	Renewable biochar derived from mixed sewage sludge and pine sawdust for carbon dioxide capture. Environmental Pollution, 2022, 306, 119399.	7.5	25
166	Growth, Structures, and Properties of Li ₂ Zn ₂ (MoO ₄) ₃ and Co-doped Li ₂ Zn ₂ (MoO ₄) ₃ . Crystal Growth and Design, 2009, 9, 914-920.	3.0	24
167	Investigation of lead(II) uptake by Bacillus thuringiensis 016. World Journal of Microbiology and Biotechnology, 2015, 31, 1729-1736.	3.6	24
168	Sulfate-reducing bacteria in anaerobic bioprocesses: basic properties of pure isolates, molecular quantification, and controlling strategies. Environmental Technology Reviews, 2018, 7, 46-72.	4.3	24
169	Synergistic chromium(VI) reduction and phenol oxidative degradation by FeS2/FeO and persulfate. Chemosphere, 2021, 281, 130957.	8.2	24
170	Effect of chromate action on morphology of basalt-inhabiting bacteria. Materials Science and Engineering C, 2006, 26, 610-612.	7.3	23
171	Direct Formation of Reusable TiO ₂ /CoFe ₂ O ₄ Heterogeneous Photocatalytic Fibers via Two-Spinneret Electrospinning. Journal of Nanoscience and Nanotechnology, 2012, 12, 2496-2502.	0.9	23
172	Potassiumâ€lon Batteries: Surface Amorphization of Vanadium Dioxide (B) for Kâ€lon Battery (Adv. Energy) Tj E	TQq0,00 r	gBT /Overloc
173	Removal of As(V) by iron-based nanoparticles synthesized via the complexation of biomolecules in green tea extracts and an iron salt. Science of the Total Environment, 2021, 764, 142883.	8.0	23
174	Rational construction of covalent organic frameworks with multi-site functional groups for highly efficient removal of low-concentration U(<scp>vi</scp>) from water. Environmental Science: Nano, 2021, 8, 1469-1480.	4.3	23
175	Boosting CO ₂ electroreduction towards C ₂₊ products <i>via</i> CO* intermediate manipulation on copper-based catalysts. Environmental Science: Nano, 2022, 9, 911-953.	4.3	23
176	In situ atomic force microscopy measurement of the dynamic variation in the elastic modulus of swollen chitosan/gelatin hybrid polymer network gels in media of different pH. Polymer International, 1999, 48, 794-798.	3.1	22
177	Nanocrystal growth via oriented attachment. CrystEngComm, 2014, 16, 1407.	2.6	22
178	Nano-Mg(OH)2-induced proliferation inhibition and dysfunction of human umbilical vein vascular endothelial cells through caveolin-1-mediated endocytosis. Cell Biology and Toxicology, 2015, 31, 15-27.	5.3	22
179	A novel multi-reaction model for kinetics of Zn release from soils: Roles of soil binding sites. Journal of Colloid and Interface Science, 2018, 514, 146-155.	9.4	22
180	Alkyne-Functionalized Ruthenium Nanoparticles: Impact of Metal–Ligand Interfacial Bonding	11.2	22

Alkyne-Functionalized Ruthenium Nanoparticles: Impact of Metala€"Ligand Interfacial Bo Interactions on the Selective Hydrogenation of Styrene. ACS Catalysis, 2019, 9, 98-104. aing 180

#	Article	IF	CITATIONS
181	Heterooctanuclear Cluster Complex Formation with Phosphine Participation:Â Synthesis, Structure, and Magnetic Properties of Co6Ru2(mp)10(PBun3)6(H2mp = 2-Mercaptophenol, PBun3=) Tj ETQq1 1 0.7843	314 rg B @ /Оvе	erlæak 10 Tf
182	Atomic Force Microscopy Analysis of Intermediates in Cobalt Hexammine-Induced DNA Condensation. Journal of Biomolecular Structure and Dynamics, 2000, 18, 1-9.	3.5	21
183	Facile in vitro hydroxyapatite remineralization of human enamel with remarkable hardness. CrystEngComm, 2013, 15, 4351.	2.6	21
184	Temperature-sensitive growth kinetics and photoluminescence properties of CdS quantum dots. CrystEngComm, 2013, 15, 4963.	2.6	21
185	Improving the electrostatic precipitation removal efficiency by desulfurized wastewater evaporation. RSC Advances, 2016, 6, 113703-113711.	3.6	21
186	Facile Fabrication of Nickel/Heazlewoodite@Carbon Nanosheets and their Superior Catalytic Performance of 4â€Nitrophenol Reduction. ChemCatChem, 2018, 10, 4143-4153.	3.7	21
187	NaCl recovery from organic pollutants-containing salt waste via dual effects of aqueous two-phase systems (ATPS) and crystal regulation with acetone. Journal of Cleaner Production, 2020, 260, 121044.	9.3	21
188	Analysis of the characteristics of phosphine production by anaerobic digestion based on microbial community dynamics, metabolic pathways, and isolation of the phosphate-reducing strain. Chemosphere, 2021, 262, 128213.	8.2	21
189	Microwave-enhanced reductive immobilization of high concentrations of chromium in a field soil using iron polysulfide. Journal of Hazardous Materials, 2021, 418, 126293.	12.4	21
190	Diversity of Microbial Community in Shihongtan Sandstone-Type Uranium Deposits, Xinjiang, China. Geomicrobiology Journal, 2012, 29, 255-263.	2.0	20
191	Heterogeneous Condensation of Water on the Mica (001) Surface: A Molecular Dynamics Simulation Work. Journal of Physical Chemistry C, 2017, 121, 6813-6819.	3.1	20
192	Simultaneous oxidation of Cr(III) and extraction of Cr(VI) from chromite ore processing residue by silicate-assisted hydrothermal treatment. Chemical Engineering Journal, 2019, 371, 565-574.	12.7	20
193	Physicochemical and environmental properties of arsenic sulfide sludge from copper and leadâ^'zinc smelter. Transactions of Nonferrous Metals Society of China, 2020, 30, 1943-1955.	4.2	20
194	Selective recovery of Cr from electroplating nanosludge <i>via</i> crystal modification and dilute acid leaching. Environmental Science: Nano, 2020, 7, 1593-1601.	4.3	20
195	Immobilized Co2+ and Cu2+ induced structural change of layered double hydroxide for efficient heterogeneous degradation of antibiotic. Journal of Hazardous Materials, 2021, 403, 123554.	12.4	20
196	Effective separation and recovery of Zn, Cu, and Cr from electroplating sludge based on differential phase transformation induced by chlorinating roasting. Science of the Total Environment, 2022, 820, 153260.	8.0	20
197	Preparation and characterization of polyoxometalate–Ag nanoparticles composite multilayer films. Thin Solid Films, 2011, 519, 2317-2322.	1.8	19
198	One-pot synthesis of nitrogen-enriched carbon spheres for hexavalent chromium removal from aqueous solution. RSC Advances, 2016, 6, 33055-33062.	3.6	19

#	Article	IF	CITATIONS
199	Research progress in the environmental application of magnesium hydroxide nanomaterials. Surfaces and Interfaces, 2020, 21, 100701.	3.0	19
200	Efficient upcycling electroplating sludge and waste PET into Ni-MOF nanocrystals for the effective photoreduction of CO ₂ . Environmental Science: Nano, 2021, 8, 390-398.	4.3	19
201	Reaction of transition metal thiolato units V. Formation of a binuclear mercury(II) complex with the dithiolato ligand i-mnt (1,1-dicyanoethylene-2,2-dithiolate). Polyhedron, 1998, 17, 2497-2502.	2.2	18
202	ZnO nanowires array grown on Ga-doped ZnO single crystal for dye-sensitized solar cells. Scientific Reports, 2015, 5, 11499.	3.3	18
203	Mechanisms of Synergistic Removal of Low Concentration As(V) by nZVI@Mg(OH) ₂ Nanocomposite. Journal of Physical Chemistry C, 2017, 121, 21411-21419.	3.1	18
204	Debromination of polybrominated biphenyls (PBBs) by zero valent metals and iron-based bimetallic particles: Mechanisms, pathways and predicting descriptor. Chemical Engineering Journal, 2018, 351, 773-781.	12.7	18
205	Removal and recovery of Pb from wastewater through a reversible phase transformation process between nano-flower-like Mg(OH) ₂ and soluble Mg(HCO ₃) ₂ . Environmental Science: Nano, 2019, 6, 467-477.	4.3	18
206	Enhanced adsorption of arsenate by spinel zinc ferrite nano particles: Effect of zinc content and site occupation. Journal of Environmental Sciences, 2019, 79, 248-255.	6.1	18
207	Simultaneous immobilization of multi-metals in a field contaminated acidic soil using carboxymethyl-cellulose-bridged nano-chlorapatite and calcium oxide. Journal of Hazardous Materials, 2021, 407, 124786.	12.4	18
208	Ultrastrong Anion Affinity of Anionic Clay Induced by Its Inherent Nanoconfinement. Environmental Science & Technology, 2021, 55, 930-940.	10.0	18
209	Surface microstructure engenders unusual hydrophobicity in phyllosilicates. Chemical Communications, 2018, 54, 5418-5421.	4.1	17
210	The immobilization mechanism of U(VI) induced by Bacillus thuringiensis 016 and the effects of coexisting ions. Biochemical Engineering Journal, 2019, 144, 57-63.	3.6	17
211	Construction of heterostructured NiFe ₂ O ₄ -C nanorods by transition metal recycling from simulated electroplating sludge leaching solution for high performance lithium ion batteries. Nanoscale, 2020, 12, 13398-13406.	5.6	17
212	Lattice-strained nanotubes facilitate efficient natural sunlight-driven CO2 photoreduction. Nano Research, 2021, 14, 2558-2567.	10.4	17
213	Highly efficient adsorption of chromium on N, S-codoped porous carbon materials derived from paper sludge. Science of the Total Environment, 2022, 834, 155312.	8.0	17
214	Relationship between the coprecipitation mechanism, doping structure and physical properties of Zn1â^'xCoxS nanocrystallites. Nanotechnology, 2007, 18, 035705.	2.6	16
215	Surface-Mediated Chromate-Resistant Mechanism ofEnterobacter CloacaeBacteria Investigated by Atomic Force Microscopy. Langmuir, 2007, 23, 4480-4485.	3.5	16
216	Formation and Self-Assembly of Cadmium Hydroxide Nanoplates in Molten Composite-Hydroxide Solution. Crystal Growth and Design, 2010, 10, 4285-4291.	3.0	16

#	Article	IF	CITATIONS
217	Nonreductive biomineralization of uranium by Bacillus subtilis ATCC–6633 under aerobic conditions. Journal of Environmental Radioactivity, 2019, 208-209, 106027.	1.7	16
218	Convenient fabrication of a core–shell Sn@TiO ₂ anode for lithium storage from tinplate electroplating sludge. Chemical Communications, 2020, 56, 10187-10190.	4.1	16
219	Separation of lattice-incorporated Cr(<scp>vi</scp>) from calcium carbonate by converting microcrystals into nanocrystals <i>via</i> the carbonation pathway based on the density functional theory study of incorporation energy. Environmental Science: Nano, 2022, 9, 1617-1626.	4.3	16
220	Highly efficient photocatalytic degradation of the emerging pollutant ciprofloxacin <i>via</i> the rational design of a magnetic interfacial junction of mangosteen peel waste-derived 3D graphene hybrid material. Environmental Science: Nano, 2022, 9, 1298-1314.	4.3	16
221	Crystal regulation of gypsum via hydrothermal treatment with hydrogen ion for Cr(VI) extraction. Journal of Hazardous Materials, 2020, 390, 120614.	12.4	15
222	Fe(II)-induced transformation of Jarosite residues generated from zinc hydrometallurgy: Influence on metals behaviors during acid washing. Hydrometallurgy, 2021, 200, 105523.	4.3	15
223	Subsolidus phase relations in the ZnO–MoO3–B2O3, ZnO–MoO3–WO3 and ZnO–WO3–B2O3 tern systems. Journal of Alloys and Compounds, 2008, 458, 144-150.	ary 5.5	14
224	Study on the influence of lattice integrity and phase composition to the photocatalytic efficiency of ZnS material. Nanoscale, 2011, 3, 1512.	5.6	14
225	Enhanced removal of zinc and cadmium from water using carboxymethyl cellulose-bridged chlorapatite nanoparticles. Chemosphere, 2021, 263, 128038.	8.2	14
226	Novel nitrogen-doped KFeS ₂ /C composites for the efficient removal of Cr(<scp>vi</scp>). Environmental Science: Nano, 2021, 8, 1057-1066.	4.3	14
227	Treatment of Cr(VI)-containing nanowastes via the growth of nanomaterial. Science Bulletin, 2010, 55, 373-377.	1.7	13
228	Simultaneous separation and immobilization of Cr(VI) from layered double hydroxide via reconstruction of the key phases. Journal of Hazardous Materials, 2021, 416, 125807.	12.4	13
229	C-Doped KNbO ₃ single crystals for enhanced piezocatalytic intermediate water splitting. Environmental Science: Nano, 2022, 9, 1952-1960.	4.3	13
230	Robust route to photocatalytic nitrogen fixation mediated by capitalizing on defect-tailored InVO ₄ nanosheets. Environmental Science: Nano, 2022, 9, 1996-2005.	4.3	13
231	Subsolidus phase relation in the system ZnO–Li2O–MoO3. Journal of Alloys and Compounds, 2007, 430, 67-70.	5.5	12
232	The Mass Production of ZnS Nanoarchitecture via Thermodynamic Design. Crystal Growth and Design, 2008, 8, 2324-2328.	3.0	12
233	The pH-dependent binding of zinc citrate to bipy/phen (bipy=2,2-bipyridine, phen=1,10-phenanthroline). Journal of Molecular Structure, 2010, 966, 59-63.	3.6	12
234	Understanding the Occurrence of the Maximum Band-Edge Photoluminescence of TGA-Capped CdS QDs via Growth Kinetic Study. Crystal Growth and Design, 2013, 13, 5220-5228.	3.0	12

#	Article	IF	CITATIONS
235	<i>In situ</i> controlled synthesis of porous Fe–N–C materials from oily sludge by chlorinating calcination and their novel application in supercapacitors. Environmental Science: Nano, 2020, 7, 3814-3823.	4.3	12
236	Cellulose Mediated Reduction and Immobilization of Cr(VI) in Chromite Ore Processing Residue. Journal of Hazardous Materials, 2020, 394, 122538.	12.4	12
237	Efficient extraction of slowly-released Cr(<scp>vi</scp>) from nano-sized ion channels in Cr(<scp>vi</scp>)–ettringite from reduced chromite ore processing residue. Environmental Science: Nano, 2020, 7, 1082-1091.	4.3	12
238	Lattice-strained nickel hydroxide nanosheets for the boosted diluted CO ₂ photoreduction. Environmental Science: Nano, 2021, 8, 2360-2371.	4.3	12
239	Spatially separated oxygen vacancies and nickel sites for ensemble promotion of selective CO2 photoreduction to CO. Cell Reports Physical Science, 2022, 3, 100724.	5.6	12
240	Specific Detection of Alpha-Fetoprotein Using AlGaAs/GaAs High Electron Mobility Transistors. IEEE Electron Device Letters, 2014, 35, 333-335.	3.9	11
241	Mechanism of dry detoxification of chromium slag by carbon monoxide. Environmental Chemistry Letters, 2019, 17, 1375-1381.	16.2	11
242	The algicidal efficacy and the mechanism of Enterobacter sp. EA-1 on Oscillatoria dominating in aquaculture system. Environmental Research, 2021, 197, 111105.	7.5	11
243	Evaluation of Phase, Microstructure and Composition of Human Dentine After Er, Cr:YSGG Laser Irradiation. Journal of Nanoscience and Nanotechnology, 2011, 11, 2421-2426.	0.9	10
244	The "jump of size―phenomenon in aqueous-nanoparticle reaction system: phase transformation from nano-Mg(OH)2 to bulk MgCO3·3H2O. CrystEngComm, 2012, 14, 7165.	2.6	10
245	Self-assembly of SnO ₂ quantum dots into hierarchically ordered structures assisted by oriented attachment. Physical Chemistry Chemical Physics, 2015, 17, 4845-4848.	2.8	10
246	Investigation of Methylene Blue Biosorption and Biodegradation by Bacillus thuringiensis 016. Water, Air, and Soil Pollution, 2015, 226, 1.	2.4	10
247	Mechanism of adsorption affinity and capacity of Mg(OH) ₂ to uranyl revealed by molecular dynamics simulation. RSC Advances, 2016, 6, 31507-31513.	3.6	10
248	Understanding and controlling the key phase transformation for selective extracting Ni and Cu from Cr-containing electroplating sludge. Surfaces and Interfaces, 2021, 24, 101090.	3.0	10
249	Efficient immobilization and utilization of chromite ore processing residue via hydrothermally constructing spinel phase Fe2+(Cr3+X, Fe3+2-x)O4 and its magnetic separation. Science of the Total Environment, 2022, 813, 152637.	8.0	10
250	Phosphine-participated formation and crystal structures of nickel complexes with 2-sulfanylphenol and phosphine ligands. Journal of the Chemical Society Dalton Transactions, 1996, , 177.	1.1	9
251	Effect of Cu(II) on the stability of oxyanion-substituted schwertmannite. Environmental Science and Pollution Research, 2018, 25, 15492-15506.	5.3	9
252	Hydrothermal alkaline conversion of sewage sludge: optimization of process parameters and characterization of humic acid. Environmental Science and Pollution Research, 2021, 28, 57695-57705.	5.3	9

#	Article	IF	CITATIONS
253	The efficient biomineralization and adsorption of cadmium (Cd2+) using secretory organo-biominerals (SOBs) produced by screened Alcaligenes faecalis K2. Environmental Research, 2021, 199, 111330.	7.5	9
254	One-step removal of high-concentration arsenic from wastewater to form Johnbaumite using arsenic-bearing gypsum. Journal of Hazardous Materials, 2022, 424, 127585.	12.4	9
255	Mechanisms of Pb(II) coprecipitation with natrojarosite and its behavior during acid dissolution. Journal of Environmental Sciences, 2022, 122, 128-137.	6.1	9
256	The ternary system Na2O–ZnO–WO3: Compounds and phase relationships. Journal of Alloys and Compounds, 2008, 458, 138-143.	5.5	8
257	The Analysis of the Immobilization Mechanism of Ni(II) on <i>Bacillus cereus</i> . Journal of Nanoscience and Nanotechnology, 2011, 11, 3597-3603.	0.9	8
258	Carbon Cloth Supported Nano-Mg(OH)2 for the Enrichment and Recovery of Rare Earth Element Eu(III) From Aqueous Solution. Frontiers in Chemistry, 2018, 6, 118.	3.6	8
259	Photocatalytic degradation of polybrominated biphenyls (PBBs) on metal doped TiO ₂ nanocomposites in aqueous environments: mechanisms and solution effects. Environmental Science: Nano, 2019, 6, 1111-1120.	4.3	8
260	Recent advances in metal/ceria catalysts for air pollution control: mechanism insight and application. Environmental Science: Nano, 2021, 8, 2760-2779.	4.3	8
261	Microinteraction Analysis between Heavy Metals and Coexisting Phases in Heavy Metal Containing Solid Wastes. ACS ES&T Engineering, 2022, 2, 547-563.	7.6	8
262	Visualization of the intermediates in a uniform DNA condensation system by tapping mode atomic force microscopy. Surface and Interface Analysis, 2001, 32, 15-19.	1.8	7
263	Subsolidus phase relations in the systems K2O–ZnO–AO3 (A=Mo, W). Journal of Alloys and Compounds, 2008, 452, 263-267.	5.5	7
264	Photocatalytic Bactericidal Mechanism of Nanoscale TiO ₂ Films on <i>Escherichia coli</i> . Journal of Nanoscience and Nanotechnology, 2011, 11, 7621-7626.	0.9	7
265	Aggregation-based abrupt crystallization from amorphous Ag ₂ S to Ag ₂ S nanocrystals. Chemical Communications, 2015, 51, 6141-6144.	4.1	7
266	Role of sulfur atoms in the adsorption of antimony by greigite. Surfaces and Interfaces, 2020, 20, 100584.	3.0	7
267	Spontaneous separation of Pb from PbSO4-coprecipitated jarosite using freeze-thaw cycling with thiourea. Transactions of Nonferrous Metals Society of China, 2022, 32, 1019-1030.	4.2	7
268	Reaction of sulfur-containing structural units of transition metals. Science in China Series B: Chemistry, 1997, 40, 634-642.	0.8	6
269	X-ray photoelectron studies of spin-state changes in 3d metal systems. Surface and Interface Analysis, 2001, 32, 114-116.	1.8	6
270	Resonant slot antennas as transducers of DNA hybridization: a computational feasibility study. , 0, , .		6

#	Article	IF	CITATIONS
271	Hydrothermal growth of large-size UO ₂ nanoparticles mediated by biomass and environmental implications. RSC Advances, 2014, 4, 62476-62482.	3.6	6
272	Growth kinetics study revealing the role of the MPA capping ligand on adjusting the growth modes and PL properties of CdTe QDs. CrystEngComm, 2014, 16, 1547-1552.	2.6	6
273	Extraction of Cr(VI) from chromite ore processing residue via hydrothermal-assisted phase transformation. Chinese Chemical Letters, 2020, 31, 1956-1960.	9.0	6
274	Identification of the active site during CF ₄ hydrolytic decomposition over γ-Al ₂ O ₃ . Environmental Science: Nano, 2022, 9, 954-963.	4.3	6
275	Upcycling of electroplating sludge into Fe3C-decorated N,P dual-doped porous carbon via microalgae as efficient sulfur host for lithium–sulfur batteries. Surfaces and Interfaces, 2022, 30, 101869.	3.0	6
276	Minimizing Fe-Bearing Waste Guided by Modulating the Precipitation Pathway: A Novel Magnetite Precipitation Approach for Zinc Hydrometallurgy. ACS ES&T Engineering, 2022, 2, 1611-1618.	7.6	6
277	Synthesis and Characterization of Nanocrystalline GaN by Ammonothermal Method Using CsNH ₂ as Mineralizer. Journal of Nanoscience and Nanotechnology, 2010, 10, 5741-5745.	0.9	5
278	Subsolidus phase relations in the ZnO–P2O5–WO3 system. Journal of Alloys and Compounds, 2010, 496, 105-109.	5.5	5
279	The relationship between photoluminescence (PL) decay and crystal growth kinetics in thioglycolic acid (TGA) capped CdTe quantum dots (QDs). Physical Chemistry Chemical Physics, 2014, 16, 11747.	2.8	5
280	Specific detection of mercury(II) irons using AlGaAs/InGaAs high electron mobility transistors. Journal of Crystal Growth, 2015, 425, 381-384.	1.5	5
281	Study on Photocatalytic Degradation of 2,4-Dichlorophenol by ZnS Microsphere. Journal of Nanoscience and Nanotechnology, 2016, 16, 1060-1066.	0.9	5
282	Preparation of Graphene ―Like Carbon Composites (GCC) by Hummers Method Using Fly Ash as Carbon Source and Its Removal of Lead from Wastewater. ChemistrySelect, 2020, 5, 6828-6833.	1.5	5
283	An Overlooked Natural Hydrogen Evolution Pathway: Ni ²⁺ Boosting H ₂ O Reduction by Fe(OH) ₂ Oxidation during Lowâ€Temperature Serpentinization. Angewandte Chemie, 2021, 133, 24256-24260.	2.0	5
284	Synthesis of Flaky Flame-retardant Magnesium Hydroxide with High Dispersion. Acta Chimica Sinica, 2012, 70, 2045.	1.4	5
285	Towards a broad-operation window for stable CO ₂ electroreduction to HCOOH by a design involving upcycling electroplating sludge-derived Sn@N/P-doped carbon. Environmental Science: Nano, 2022, 9, 511-522.	4.3	5
286	AFM as a surface probe—beyond structural information. Surface and Interface Analysis, 1999, 28, 44-48.	1.8	4
287	Surface Treatment to Enhance Photocatalytic Activity of ZnS Complex Nanostructure via a Post-Synthesis Route. Journal of Nanoscience and Nanotechnology, 2009, 9, 6721-6725.	0.9	4
288	<i>In Situ</i> Conversion of ZnO Microsphere from ZnS Complex Microstructure and Photocatalytic Study. Journal of Nanoscience and Nanotechnology, 2012, 12, 7371-7375.	0.9	4

#	Article	IF	CITATIONS
289	Al-doped ZnO thin film enhancing the photo-catalytic bactericidal performance on the (100) plane of ZnO single crystal. Catalysis Today, 2014, 224, 188-192.	4.4	4
290	Immobilization of Uranium at Nanoscale by <i>Bacillus cereus</i> 12-2 at Different U(VI) Concentration. Journal of Nanoscience and Nanotechnology, 2019, 19, 7131-7138.	0.9	4
291	Substitution-mediated enhanced adsorption of low concentration As(<scp>v</scp>) from water by mesoporous Mn _x Fe _{3â^'x} O ₄ microspheres. Environmental Science: Nano, 2019, 6, 1406-1417.	4.3	4
292	Interaction of pyrite with zerovalent iron with superior reductive ability <i>via</i> Fe(<scp>ii</scp>) regeneration. Environmental Science: Nano, 2022, 9, 2713-2725.	4.3	4
293	Surface morphology studies of in situ polycondensation microcomposites using atomic force microscopy. Applied Physics A: Materials Science and Processing, 1998, 66, S591-S596.	2.3	3
294	Investigation of various structures of DNA molecules (III). Science in China Series C: Life Sciences, 1999, 42, 136-140.	1.3	3
295	REACTIONS OF TRANSITION METAL THIOLATO UNITS IV. FORMATION OF PHOSPHINE-CONTAINING COBALT OR NICKEL COMPLEXES WITH iso-MALEONITRILE-DITHIOLATE. Journal of Coordination Chemistry, 1999, 46, 409-424.	2.2	3
296	Improved Removal of Cr(VI) using Fe 3 O 4 /C Magnetic Nanocomposites Derived from Potassium Fulvic Acid. ChemistrySelect, 2019, 4, 13656-13662.	1.5	3
297	Investigation on the treatment of Cr(VI) by Bacillus cereus 12-2 under metal cation. Surfaces and Interfaces, 2021, 24, 101141.	3.0	3
298	Evaluation of three common alkaline agents for immobilization of multi-metals in a field-contaminated acidic soil. Environmental Science and Pollution Research, 2021, 28, 60765-60777.	5.3	3
299	Atomic force microscopy observation of the condensates of the spermidine-DNA complexes. Science in China Series B: Chemistry, 1998, 41, 418-423.	0.8	2
300	Intermolecular forces between acetylcholine and acetylcholinesterases studied with atomic force microscopy. Science in China Series B: Chemistry, 1999, 42, 449-457.	0.8	2
301	Visualization of reconstituted solenoid chromatin structure by tapping mode atomic force microscopy. Surface and Interface Analysis, 2001, 32, 20-26.	1.8	2
302	Intrinsic magnetism of a series of Co substituted ZnO single crystals. Journal of Physics Condensed Matter, 2008, 20, 035206.	1.8	2
303	Large Verdet constant in the Tb implanted gamma-Fe 2 O 3 films. Thin Solid Films, 2014, 571, 45-50.	1.8	2
304	Facile Preparation of Super Absorbent from Calcium–Aluminum Waste Residue and Its Application for Adsorption of Congo Red. Journal of Nanoscience and Nanotechnology, 2020, 20, 769-778.	0.9	2
305	Bio-inspired hydrogen-bond network for extraction of organometal micropollutants from water. Cell Reports Physical Science, 2021, 2, 100625.	5.6	2
306	Quaternary amine synthesized ionic polymer for efficient removal of Cr(VI) in waste water. Surfaces and Interfaces, 2021, 23, 101031.	3.0	1

#	Article	IF	CITATIONS
307	The Cytotoxicity of NiO Nanoparticle with Borate Capping. Journal of Nanoscience and Nanotechnology, 2011, 11, 10142-10148.	0.9	Ο
308	Regulating the Formation of Self-Supported LiCoO ₂ Nanostructure by Alkaline Concentration and Study on Its Electrochemical Property. Journal of Nanoscience and Nanotechnology, 2014, 14, 3919-3924.	0.9	0
309	Understanding and controlling the key crystal phase transformation for recovery of sodium chloride from organic waste salt. Surfaces and Interfaces, 2021, 27, 101499.	3.0	0
310	Accelerated Degradation of Microplastics at the Liquid Interface of Ice Crystals in Frozen Aqueous Solutions. Angewandte Chemie, 0, , .	2.0	0